

Hybrid systems for the generation of non-classical mechanical states via quadratic interactions: Supplemental Material

Carlos Sánchez Muñoz,^{1,*} Antonio Lara,² Jorge Puebla,¹ and Franco Nori^{1,3}

¹Theoretical Quantum Physics Laboratory, Cluster for Pioneering Research, RIKEN, Saitama, 351-0198, Japan

²Dpto. Física Materia Condensada C03, Instituto Nicolas Cabrera (INC),

Condensed Matter Physics Institute (IFIMAC), Universidad Autónoma de Madrid, 28049, Madrid, Spain

³Department of Physics, University of Michigan, Ann Arbor, MI 48109-1040, USA

(Dated: August 28, 2018)

I. MAGNETIC FIELD SIMULATIONS

For the case of Dy, we have considered a saturation magnetization of $\mu_0 M_s = 3.7$ T [1], exchange stiffness $A = 1.5 \times 10^{-12}$ Jm⁻¹ [2], and a magnetic damping $\alpha = 0.036$ [3]; for Co, we take $\mu_0 M_s = 1.79$ T [4], $A = 3.1 \times 10^{-11}$ Jm⁻¹ [5] and $\alpha = 0.005$ [6]; and for FeCo, $\mu_0 M_s = 2.4$ T [6], $A = 1.7 \times 10^{-11}$ Jm⁻¹ [7] and $\alpha = 10^{-4}$ [6]. Note that, regarding the fabrication of these nanopillars, outstanding control on the size and shape can be achieved by using a variety of techniques, such as molecular beam epitaxy [8] or focused electron-beam-induced deposition (FEUID) [9]. We calculated the magnetic field generated by the cylinders using MuMax3 [10], a finite differences, open-source solver of the Landau-Lifshitz-Gilbert equation [11].

II. MASTER EQUATION AND QUANTUM TRAJECTORY SIMULATIONS

Simulation of the system dynamics in a dissipative environment has been performed following two different techniques:

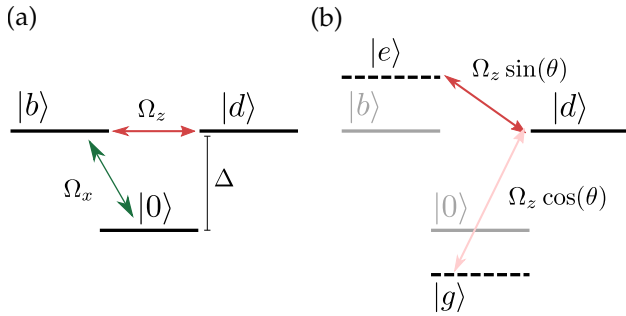


FIG. S1. Procedure to obtain an effective TLS. (a) Bare energy levels defined in the basis of bright and dark states and in the frame rotating with ω_x , see Eq. (S4). $|b\rangle$ is coupled to $|0\rangle$ through the microwave magnetic field in the x axis, and to $|d\rangle$ through the magnetic field in the z axis. (b) The microwave field dresses the states $|b\rangle$ and $|0\rangle$. In the basis of dressed energy levels, the states $|e\rangle$ and $|d\rangle$ define an effective TLS, driven by the field in z axis. If $\Delta \gg \Omega_x$, $\sin(\theta) \approx 1$.

master equation simulations and the method of quantum trajectories.

For the master equation simulations, we solved numerically the differential equations that govern the evolution of the density matrix:

$$\dot{\rho} = -i[H, \rho] + (\gamma_m n_{\text{th}}/2) \mathcal{L}_a[\rho] + (\gamma_z/2) \mathcal{L}_{\sigma^{\dagger}\sigma}[\rho], \quad (\text{S1})$$

where $\mathcal{L}_O[\rho] \equiv 2O\rho O^{\dagger} - O^{\dagger}O\rho - \rho O^{\dagger}O$. This was done by truncating the Hilbert space setting a maximum number N of phonons in the oscillator. For the calculations done in this manuscript, $N = 100$ was enough to guarantee convergence for the highest values of driving considered.

The method of quantum trajectories yields a stochastic evolution of a pure wavefunction, which averaged over many different realizations provides the same predictions as the master equation for the density matrix. At every finite time step dt , for each element of the type $(\gamma_i/2) \mathcal{L}_{O_i}[\rho]$ in the master equation, the wavefunction $|\psi(t)\rangle$ can randomly undergo a quantum jump with probability $p_i = \gamma_i \langle \psi(t) | O_i | \psi(t) \rangle dt$ that transforms the system as

$$|\psi(t+dt)\rangle \propto O_i |\psi(t)\rangle \quad (\text{S2})$$

(under proper normalization). The occurrence of a jump is determined by generating a random number $r_i \in [0, 1]$ at each time step, so that the jump occurs whenever $r < p_i$ (dt must be chosen small enough so that, at every time step, $p_i \ll 1$). When no jump occurs, the wavefunction evolves as

$$|\psi(t+dt)\rangle \propto e^{-iH_{\text{eff}} dt} |\psi(t)\rangle, \quad (\text{S3})$$

where H_{eff} is a non-Hermitian Hamiltonian, $H_{\text{eff}} \equiv H - i \sum_i (\gamma_i/2) O_i^{\dagger} O_i$.

III. DERIVATION OF THE TWO-PHONON, DRIVEN JAYNES-CUMMINGS HAMILTONIAN

Here we define an effective TLS in a way very similar to the one outlined in Refs. [12, 13]. Our starting point is the Hamiltonian:

$$H = DS_z^2 + \Omega_x \cos(\omega_x t) S_x + \Omega_z \cos(\omega_z t) S_z + \omega_m a^{\dagger} a + g_2 (a^{\dagger} + a)^2 S_z. \quad (\text{S4})$$

* Present address: Clarendon Laboratory, University of Oxford, Oxford OX1 3PU, UK

By working in the basis of bright and dark states

$$|b\rangle = \frac{1}{\sqrt{2}}(|-1\rangle + |1\rangle), \quad (\text{S5})$$

$$|d\rangle = \frac{1}{\sqrt{2}}(|-1\rangle - |1\rangle), \quad (\text{S6})$$

and assuming, $\Omega_x \ll \omega_x \sim D$, we can perform a rotating wave approximation and apply a unitary transformation $U = \exp[i\omega_x t(|b\rangle\langle b| + |d\rangle\langle d|)]$ to Eq. (S4) in order to move to a rotating frame where the time dependence with ω_x is eliminated:

$$H = \Delta(|b\rangle\langle b| + |d\rangle\langle d|) + \omega_m a^\dagger a + [\Omega_x |0\rangle\langle b| + \Omega_z \cos(\omega_z t) |b\rangle\langle d| + g_2(a^\dagger + a)^2 |b\rangle\langle d| + \text{h.c.}], \quad (\text{S7})$$

with $\Delta \equiv D - \omega_x$. The driving term with Ω_x can be removed by working in the dressed basis of states $|g\rangle$ and $|e\rangle$:

$$|g\rangle = \sin(\theta) |0\rangle - \cos(\theta) |b\rangle, \quad (\text{S8})$$

$$|e\rangle = \cos(\theta) |0\rangle + \sin(\theta) |b\rangle, \quad (\text{S9})$$

with $\cos(\theta) = 1/\sqrt{1+\xi^2}$, $\sin(\theta) = \xi/\sqrt{1+\xi^2}$, and $\xi = \Omega_x/(\Delta/2 + R)$, where $R = \sqrt{\Omega_x^2 + (\Delta/2)^2}$. In the limit $\Delta \approx 0$, we have $\omega_{gd} = \omega_{de} = \Omega_x$. This makes it evident that we should take the opposite limit $\Delta \gg \Omega_x$, since this will increase the difference between ω_{gd} and ω_{de} , allowing us to spectrally isolate one of these transitions as an effective TLS. In that case, $\omega_{gd} \approx \Delta + \Omega_x^2/\Delta$, and $\omega_{de} \approx \Omega_x^2/\Delta$, so that $\omega_{gd} \gg \omega_{de}$, and $\sin(\theta) \approx 1$. By defining an effective TLS with lowering operator $\sigma \equiv |d\rangle\langle e|$ and transition energy $\omega_\sigma = \omega_{de}$, and assuming $\Omega_z \ll \omega_\sigma$, we can make a rotating wave approximation to eliminate fast-rotating terms and perform a final unitary transformation $U = \exp[i\omega_z t(\sigma^\dagger \sigma + a^\dagger a/2)]$ to remove the remaining time dependence, yielding the driven, two-phonon Jaynes-Cummings Hamiltonian of Eq. (2) in the main text. Here and in the main text, we define $\Omega \equiv \Omega_z$ to lighten the notation. The scheme presented here is sketched in Fig. S1. The derivation will be valid for $\Omega_x \ll \{\Delta, \omega_x\}$, $\Omega \ll \Omega_x$, and $g_2 \ll \omega_m$, with $\Delta \equiv D - \omega_x$. Since $D = 2\pi \times 2.88$ GHz, a sensible choice of parameters is $\omega_x = 2\pi \times 1$ GHz, giving $\Delta = 2\pi \times 1.88$ GHz. Since we want $\omega_\sigma = 2\omega_m \approx 2\pi \times 3.6$ MHz, this implies a value $\Omega_x \approx 2\pi \times 82$ MHz, which fulfills the conditions above and sets the maximum limit for the driving Ω .

IV. FIRST ORDER MAGNETIC GRADIENT EFFECTS DUE TO IMPERFECT ALIGNMENT

In the main text, we considered a geometry in which the equilibrium point of the oscillator lies exactly at the center of the gap between two nanomagnets, yielding a null first-order gradient of the magnetic field and therefore a pure quadratic coupling. However, it is important to address to which extent unavoidable deviations from a perfectly aligned situation might render noticeable effects due to the induced coupling through first-order gradients. In the simulation depicted in Fig. S2, we observe that a misalignment of 0.1 nm is able

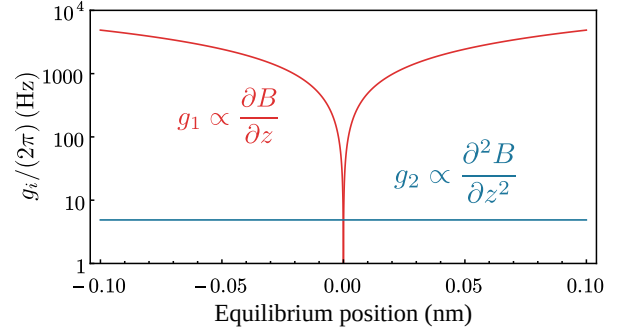


FIG. S2. First and second-order coupling rates as a function of the equilibrium position of the oscillator with respect to the center of the gap between the magnets.

to induce first-order couplings in the range of kHz. Taking into account that we are considering mechanical modes with frequencies $\omega_m \sim$ MHz and fixing the two-phonon resonant condition $\omega_\sigma \approx 2\omega_m$, we see that first-order gradient terms of the kind $g_1(a + a^\dagger)(\sigma + \sigma^\dagger)$ will rotate as $\sim \exp[\pm i\omega_m t]$ and can therefore be neglected beside unimportant frequency shifts (e.g., even for g_1 as high as 100 kHz, one can still achieve full two-phonon Rabi oscillations governed by $g_2/(2\pi) = 5$ Hz by tuning the TLS frequency to $\omega_\sigma = \omega_m - \lambda$, with $\lambda \approx 3.54$ kHz).

By tuning the TLS in resonance with the mechanical mode, $\omega_\sigma = \omega_m$, the first-order coupling can be used as well to stabilize the resonator close to the middle point. The variation in g_1 as the oscillator is moved would yield different responses of the TLS, which could be used in a feedback loop to correct the position of the resonator. It has been demonstrated that picometer stability can be achieved by adding feedback control to piezo-actuators via spectroscopy arrangements, which can be readily obtained by monitoring the NV center light emission [14, 15].

V. DETECTION OF MECHANICAL NON-CLASSICAL STATES

In the main text, we have focused on the generation of non-classical states of motion. In an experimental implementation, it is vital to have a scheme to detect and reconstruct such states. There is a great body of work regarding the reconstruction of mechanical states [16]; here, we comment on the route consisting of a displacement and a phonon number measurement. One possible way to see that this technique allows to reconstruct the quantum state is to note that the Wigner function can be written as

$$W(\alpha, \alpha^*) = 2\pi \text{Tr}\{\hat{D}^\dagger(\alpha)\hat{\rho}\hat{D}(\alpha)\hat{P}\}, \quad (\text{S10})$$

with \hat{D} the displacement operator and \hat{P} the parity operator. Through phonon number measurements, we can obtain the expected value of the parity operator for different displaced states and reconstruct the Wigner function.

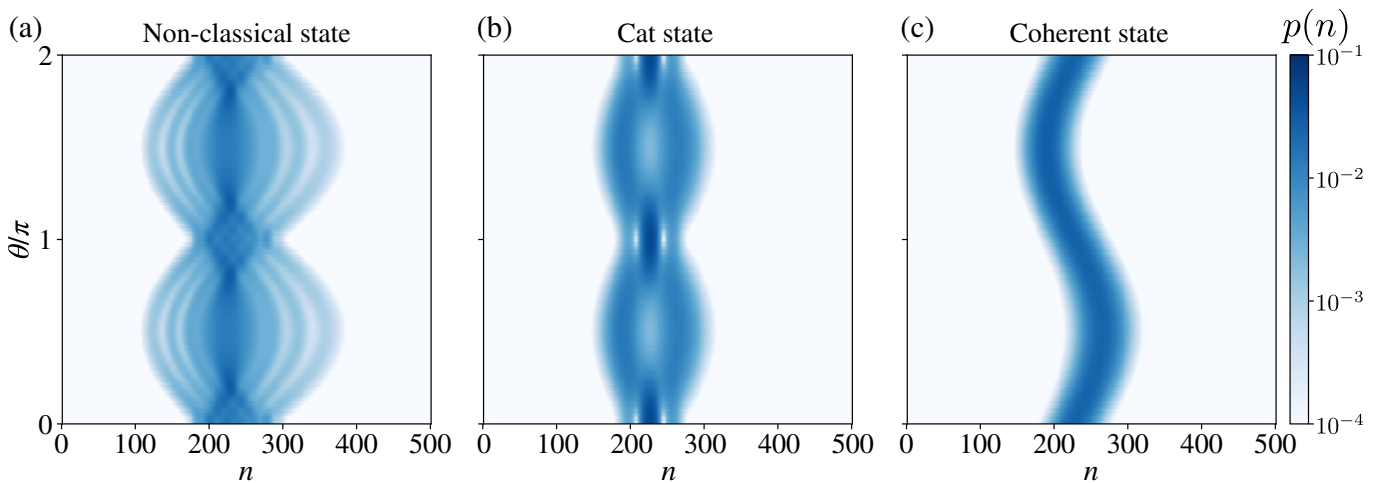


FIG. S3. Simulation of a state-reconstruction measurement. A given mechanical state is displaced by a fixed amplitude $|\alpha| = 15$ and a variable angle θ , and the phonon number distribution $p(n)$ is measured. The states used here are: (a) a non-classical mechanical state generated by our system (the same as in the inset of Fig. 5 in the main text); (b) a cat state with the same phonon population as in (a); (c) a coherent state with the same phonon population as in (a). This data can be used to retrieve the quantum state of the system via reconstruction algorithms.

We can also picture the number measurement on a displaced state as an homodyne measurement; by considering the displaced annihilation operator $\tilde{a} = a + \alpha$, with $\alpha = |\alpha|e^{i\theta}$, the resulting number operator is

$$\tilde{a}^\dagger \tilde{a} = a^\dagger a + a^\dagger \alpha + \alpha^* a + |\alpha|^2. \quad (\text{S11})$$

For $|\alpha|^2 \gg \langle a^\dagger a \rangle$, we obtain that the number measurement of the displaced state minus an offset $|\alpha|^2$ measures the quadrature amplitude Q_θ :

$$(\tilde{a}^\dagger \tilde{a} - |\alpha|^2) / (\sqrt{2}|\alpha|) \approx (ae^{-i\theta} + a^\dagger e^{i\theta}) / \sqrt{2} = Q_\theta. \quad (\text{S12})$$

Measured over one complete cycle in θ , the quadrature amplitudes Q_θ provide tomographically complete information about the quantum system [17, 18]. Figure S3 shows a simulation of the proposed measurement; a given state is displaced by a fixed amplitude α and a variable phase θ , and the phonon number distribution is measured. The difference between the resulting data for the distinct states considered is apparent even to the naked eye; this information can be used to infer the quantum state through multiple reconstruction algorithms, like maximum likelihood or entropy maximization [16].

The qubit-resonator coupling can also be used in order to perform state tomography of the mechanical oscillator. First order effects allow us to go from a resonant two-phonon coupling regime to a resonant or dispersive one-phonon coupling regime by tuning the TLS energy out of the two-phonon resonance. This would allow, for instance, to measure the state of the oscillator generated by the two-phonon interaction by suddenly switching the TLS energy to a regime of dispersive interaction governed by g_1 , which can be used to employ techniques of state reconstruction via displacement and number measurement through Ramsey interferometry of the qubit [16, 19, 20].

VI. CONFINED DYNAMICS IN PHASE SPACE

The role of nonlinearity brought by the TLS is to limit the dynamics to a region of the phase space of the oscillator. This is clearer if we represent Eq. (2) in the basis that diagonalizes the driven-TLS Hamiltonian [21], considering, for simplicity, the resonant case $\omega_\sigma = \omega_z$:

$$H = \Omega \tilde{\sigma}_z + (\omega_m - 2\omega_z) a^\dagger a + \frac{g_2}{2} [a^{\dagger 2} (\tilde{\sigma} - \tilde{\sigma}^\dagger + \tilde{\sigma}_z) + \text{h.c.}] \quad (\text{S13})$$

At high driving, $\Omega \gg g_2$, the terms proportional to $a^{\dagger 2} (\tilde{\sigma} - \tilde{\sigma}^\dagger) + \text{h.c.}$ are counter-rotating and do not contribute to the dynamics provided that $n_a g_2 \ll \Omega$, where n_a is the phonon population in the oscillator. In this case, the evolution under the terms $a^{\dagger 2} \tilde{\sigma}_z + \text{h.c.}$ is decoupled for the two eigenstates of $\tilde{\sigma}_z$, $|\pm\rangle$, and takes the form of a squeezing operation along the angle $\pm\pi/4$. Due to this squeezing operation, the phonon population of the oscillator grows. Once the population reaches a value such that $n_a g_2 \approx \Omega$, the counter-rotating terms enter into action and distort the evolution. They act as a barrier in phase space, preventing a small initial population from growing past a given threshold, in close similarity the physics of confined quantum Zeno dynamics [22–24]. This is shown in Fig. 4 in the main text, where we depict the evolution, from the moment the driving is turned on, of a system initially in its ground state. In order to gain insight in the driven-dissipative nature of the dynamics, we show the phonon population and Wigner functions of the reduced cavity system, computed both from the density matrix and from the wavefunction of a single quantum trajectory [25]. Initially, the TLS is in its ground state, which is described in the dressed basis as a linear superposition $|g\rangle \propto |+\rangle + |-\rangle$. Therefore, the mechanical mode evolves in a superposition of being squeezed along the $\pi/4$ and $-\pi/4$ axes, yielding a cross-like pattern in phase space, as shown in the first column of Fig. 4(b). After that, the counter-rotating

terms enter into action and the squeezing is distorted, yielding a ribbon-like pattern in a confined region of phase space. Finally, the interplay between the coherent evolution and dissipation in the resonator yields a steady Wigner function with two lobes associated to the coherent states $|\pm i\sqrt{\Omega/g_2}\rangle$.

VII. LONG-LIVED CATS IN A QUANTUM TRAJECTORY

When considering a single quantum trajectory, any cat state in which the system is found to be remains stable for very long times, even in the absence of any feedback protocol. The reason is that they are only affected by the random quantum jumps that flip their phase. At any time, the probability to undergo a jump during a small time interval dt is $p = \gamma_m n_{th} n_a dt$. Therefore, if the system is initialized in one of the two cat states that compose the mixed steady state, this state remains stable with a fidelity:

$$F(t) \approx 1 - \frac{1}{2} \gamma_m n_{th} n_a t, \quad (S14)$$

where we considered time intervals shorter than the phonon lifetime, i.e., $t < 1/(\gamma_m n_{th} n_a)$. Since phonon lifetimes can reach hundreds of seconds in oscillators with high quality factors [26], a cat state in this system can in fact be extremely long lived. This is shown in Fig. S4, where we selected a pure state of the quantum trajectory at a random time (once

the evolution is stationary) that is very close to a cat state, let it evolve as a mixed state under the master equation, and computed the fidelity to a cat state with the same population as the initial state. This shows that the cat state can be maintained stable in this system with a fidelity $F > 0.99$ for times ~ 1 ms, during which it can be used as a resource for quantum applications [27–31].

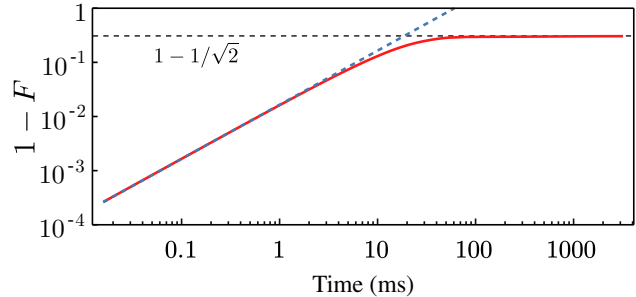


FIG. S4. Fidelity F to a cat state versus time for an initial state chosen from a random time ($t = 0$) in the quantum trajectory, once the steady-state limit is reached. The initial state resembles a cat with fidelity $F > 0.999$. The blue, dashed line corresponds to the expression for $F \approx 1 - \frac{1}{2} \gamma_m n_{th} n_a t$, which is valid for short times. For long times, the fidelity tends to $F = 1/\sqrt{2}$. Simulation parameter, those of Figs. 3-4.

-
- [1] G. Scheunert, C. Ward, W. Hendren, A. Lapicki, R. Hardeman, M. Mooney, M. Gubbins, and R. Bowman, *Influence of strain and polycrystalline ordering on magnetic properties of high moment rare earth metals and alloys*, J. Phys. D: Appl. Phys. **47**, 415005 (2014).
 - [2] P. Saraiva, A. Nogaret, J. Portal, H. Beere, and D. Ritchie, *Dipolar spin waves of lateral magnetic superlattices*, Phys. Rev. B **82**, 224417 (2010).
 - [3] G. Woltersdorf, M. Kiessling, G. Meyer, J.-U. Thiele, and C. Back, *Damping by slow relaxing rare earth impurities in Ni 80 Fe 20*, Phys. Rev. Lett. **102**, 257602 (2009).
 - [4] J. Cantu-Valle, I. Betancourt, J. E. Sanchez, F. Ruiz-Zepeda, M. M. Maqableh, F. Mendoza-Santoyo, B. J. Stadler, and A. Ponce, *Mapping the magnetic and crystal structure in cobalt nanowires*, J. Appl. Phys. **118**, 024302 (2015).
 - [5] F. Manfred *et al.*, *Micromagnetism and the microstructure of ferromagnetic solids* (Cambridge university press, 2003).
 - [6] M. A. Schoen, D. Thonig, M. L. Schneider, T. Silva, H. T. Nembach, O. Eriksson, O. Karis, and J. M. Shaw, *Ultra-low magnetic damping of a metallic ferromagnet*, Nat. Phys. **12**, 839 (2016).
 - [7] X. Liu and A. Morisako, *Soft magnetic properties of FeCo films with high saturation magnetization*, J. Appl. Phys. **103**, 07E726 (2008).
 - [8] B. Pigeau, C. Hahn, G. De Loubens, V. Naletov, O. Klein, K. Mitsuzuka, D. Lacour, M. Hehn, S. Andrieu, and F. Montaigne, *Measurement of the dynamical dipolar coupling in a pair of magnetic nanodisks using a ferromagnetic resonance force microscope*, Phys. Rev. Lett. **109**, 247602 (2012).
 - [9] M. Gavagnin, H. D. Wanzenboeck, S. Wachter, M. M. Shawrav, A. Persson, K. Gunnarsson, P. Svedlindh, M. Stoger-Pollach, and E. Bertagnoli, *Free-standing magnetic nanopillars for 3D nanomagnet logic*, ACS App. Materials & Interfaces **6**, 20254 (2014).
 - [10] A. Vansteenkiste, J. Leliaert, M. Dvornik, M. Helsen, F. Garcia-Sanchez, and B. Van Waeyenberge, *The design and verification of MuMax3*, AIP Advances **4**, 107133 (2014).
 - [11] T. L. Gilbert, *A phenomenological theory of damping in ferromagnetic materials*, IEEE Trans. Magn. **40**, 3443 (2004).
 - [12] P. Rabl, P. Cappellaro, M. G. Dutt, L. Jiang, J. Maze, and M. D. Lukin, *Strong magnetic coupling between an electronic spin qubit and a mechanical resonator*, Phys. Rev. B **79**, 041302 (2009).
 - [13] P.-B. Li, Z.-L. Xiang, P. Rabl, and F. Nori, *Hybrid quantum device with nitrogen-vacancy centers in diamond coupled to carbon nanotubes*, Phys. Rev. Lett. **117**, 015502 (2016).
 - [14] R. Walder, D. H. Paik, M. S. Bull, C. Sauer, and T. T. Perkins, *Ultraprecise measurement platform: sub-nm drift over hours in 3D at room temperature*, **23** (2015).
 - [15] T. Hümmer, J. Noe, M. S. Hofmann, T. W. Hänsch, A. Högele, and D. Hunger, *Cavity-enhanced Raman microscopy of individual carbon nanotubes*, Nat. Comm. **7**, 12155 (2016).
 - [16] M. R. Vanner, I. Pikovski, and M. Kim, *Towards optomechanical quantum state reconstruction of mechanical motion*, Annalen der Physik **527**, 15 (2015).
 - [17] A. I. Lvovsky and M. G. Raymer, *Continuous-variable optical quantum-state tomography*, Rev. Mod. Phys. **81**, 299 (2009).

- [18] K. Vogel and H. Risken, *Determination of quasiprobability distributions in terms of probability distributions for the rotated quadrature phase*, Phys. Rev. A **40**, 2847 (1989).
- [19] S. Haroche and J.-M. Raimond, *Exploring the Quantum: Atoms, Cavities, and Photons* (Oxford University Press, 2006).
- [20] S. Deleglise, I. Dotsenko, C. Sayrin, J. Bernu, M. Brune, J.-M. Raimond, and S. Haroche, *Reconstruction of non-classical cavity field states with snapshots of their decoherence*, Nature **455**, 510 (2008).
- [21] C. Sánchez Muñoz, F. P. Laussy, E. del Valle, C. Tejedor, and A. González-Tudela, *Filtering multiphoton emission from state-of-the-art cavity quantum electrodynamics*, Optica **5**, 14 (2018).
- [22] J.-M. Raimond, C. Sayrin, S. Gleyzes, I. Dotsenko, M. Brune, S. Haroche, P. Facchi, and S. Pascazio, *Phase space tweezers for tailoring cavity fields by quantum Zeno dynamics*, Phys. Rev. Lett. **105**, 213601 (2010).
- [23] J. M. Raimond, P. Facchi, B. Peaudecerf, S. Pascazio, C. Sayrin, I. Dotsenko, S. Gleyzes, M. Brune, and S. Haroche, *Quantum Zeno dynamics of a field in a cavity*, Phys. Rev. A **86**, 032120 (2012).
- [24] A. Signoles, A. Facon, D. Grosso, I. Dotsenko, S. Haroche, J.-M. Raimond, M. Brune, and S. Gleyzes, *Confined quantum Zeno dynamics of a watched atomic arrow*, Nat. Phys. **10**, 715 (2014).
- [25] M. B. Plenio and P. L. Knight, *The quantum-jump approach to dissipative dynamics in quantum optics*, Rev. Mod. Phys. **70**, 101 (1998).
- [26] A. Ghadimi, S. Fedorov, N. Engelsen, M. Beryhi, R. Schilling, D. Wilson, and T. Kippenberg, *Elastic strain engineering for ultralow mechanical dissipation*, Science **360**, 764 (2018).
- [27] T. C. Ralph, A. Gilchrist, G. J. Milburn, W. J. Munro, and S. Glancy, *Quantum computation with optical coherent states*, Phys. Rev. A **68**, 042319 (2003).
- [28] A. Lund, T. Ralph, and H. Haselgrove, *Fault-tolerant linear optical quantum computing with small-amplitude coherent states*, Phys. Rev. Lett. **100**, 030503 (2008).
- [29] J. Joo, W. J. Munro, and T. P. Spiller, *Quantum metrology with entangled coherent states*, Phys. Rev. Lett. **107**, 083601 (2011).
- [30] A. Facon, E.-K. Dietsche, D. Grosso, S. Haroche, J.-M. Raimond, M. Brune, and S. Gleyzes, *A sensitive electrometer based on a Rydberg atom in a Schrödinger-cat state*, Nature **535**, 262 (2016).
- [31] V. V. Albert, C. Shu, S. Krastanov, C. Shen, R.-B. Liu, Z.-B. Yang, R. J. Schoelkopf, M. Mirrahimi, M. H. Devoret, and L. Jiang, *Holonomic Quantum Control with Continuous Variable Systems*, Phys. Rev. Lett. **116**, 140502 (2016).